CrossMark

Bursting Bubbles: Clustered Supernova Feedback in Local and High-redshift Galaxies

Matthew E. Orr[1,2,3] , Drummond B. Fielding[2] , Christopher C. Hayward[2] , and Blakesley Burkhart[1,2]
[1] Department of Physics and Astronomy, Rutgers University, 136 Frelinghuysen Road, Piscataway, NJ 08854, USA; matt.orr@rutgers.edu
[2] Center for Computational Astrophysics, Flatiron Institute, 162 Fifth Avenue, New York, NY 10010, USA
[3] TAPIR, Mailcode 350-17, California Institute of Technology, Pasadena, CA 91125, USA

Abstract

We compare an analytic model for the evolution of supernova-driven superbubbles with observations of local and high-redshift galaxies, and the properties of intact H I shells in local star-forming galaxies. Our model correctly predicts the presence of superwinds in local star-forming galaxies (e.g., NGC 253) and the ubiquity of outflows near $z \sim 2$. We find that high-redshift galaxies may "capture" 20%–50% of their feedback momentum in the dense ISM (with the remainder escaping into the nearby CGM), whereas local galaxies may contain $\lesssim 10\%$ of their feedback momentum from the central starburst. Using azimuthally averaged galaxy properties, we predict that most superbubbles stall and fragment *within* the ISM, and that this occurs at, or near, the gas scale height. We find a consistent interpretation in the observed H I bubble radii and velocities, and predict that most will fragment within the ISM, and that those able to break out originate from short dynamical time regions (where the dynamical time is shorter than feedback timescales). Additionally, we demonstrate that models with constant star cluster formation efficiency per Toomre mass are inconsistent with the occurrence of outflows from high-z starbursts and local circumnuclear regions.

1. Introduction

Turbulence driven by supernova (SN) explosions provides a critical source of support in galaxies that helps set the disk scale height and prevents gravity from causing runaway star formation (Faucher-Giguere et al. 2013), alongside other physical processes like gas accretion onto and transport within galaxies[4] (Krumholz et al. 2018). Other forms of feedback, from stellar winds to photoionizing radiation, are important in the context of setting the *local* efficiency of star formation in molecular clouds (Dale et al. 2014; Grudić et al. 2018; Burkhart & Mocz 2019; Li et al. 2019), but are unable to affect structures on the scale of galactic disks. Therefore, in order to make sense of the turbulent structure of the ISM on the largest scales and how feedback processes drive galactic winds and fountains, a rigorous understanding of the nature and effects of SN feedback is required.

Star formation is inherently a clustered process, with stars forming hierarchically inside marginally gravitationally bound molecular clouds (Lada & Lada 2003). Star-forming clouds are also clustered temporally, only producing stars for roughly an internal freefall time, ($\sim$1–3 Myr; the clouds themselves existing for a few freefall times, $\lesssim$10 Myr), before being dispersed initially by "prompt" feedback processes, like stellar winds and photoionizing radiation, and finally by the first core-collapse SN explosions (Murray et al. 2010; Grudić et al. 2018; Li et al. 2019). As stellar explosions continue in the molecular

environment, the overlapping SN remnants can form an encompassing shock front described as a superbubble (Koo & McKee 1992).

Galaxy simulations with realistic implementations of star formation and SNe are able to reproduce observed stellar mass relations, low average star formation efficiencies, and the level of turbulence in galaxies (Agertz & Kravtsov 2016; Wetzel et al. 2016; Kim & Ostriker 2017; Hopkins et al. 2018; Pillepich et al. 2018; Orr et al. 2018, 2020). These simulations implicitly incorporate clustered SN feedback as the star formation events themselves are inherently clustered. A number of "small-box" simulations have focused on the ability of SN-driven superbubbles to drive galactic fountains and outflows (Martizzi et al. 2016; Kim & Ostriker 2017; Fielding et al. 2018), confirming that the clustering of SNe is crucial to realizing realistic ISM structure. However, until now, there has not been a robust, first-principles model of *how* clustered supernovae in galaxies regulate star formation and drive outflows, and specifically the local interstellar medium (ISM) conditions required for either.

In Orr et al. (2021), Paper I of this series, we developed an analytic model of clustered SN feedback and established the likely outcome and effects of supernova-driven superbubbles in the ISM, and on the flow of gas into and out of galaxies. We found that the local gas fraction and dynamical time in galaxies alone determine if star clusters can drive galactic winds/ outflows (the subsequent wind/outflow properties, including the ability to entrain cold material, being described by a wind-specific model like that of Fielding & Bryan 2021), with implications for the stall/fragmentation scale of superbubbles, and the effective strength of feedback in driving gas turbulence within galaxies.

In this Letter, we will compare our model from Paper I (hereafter, O21) of (spatially and temporally) clustered core-collapse SNe feedback, in the form of superbubbles expanding

---

[4] Transport processes are especially important at high redshifts $z \gtrsim 1$, when galaxies are most rapidly accreting gas and assembling their stellar populations (Behroozi et al. 2013; Krumholz et al. 2018).
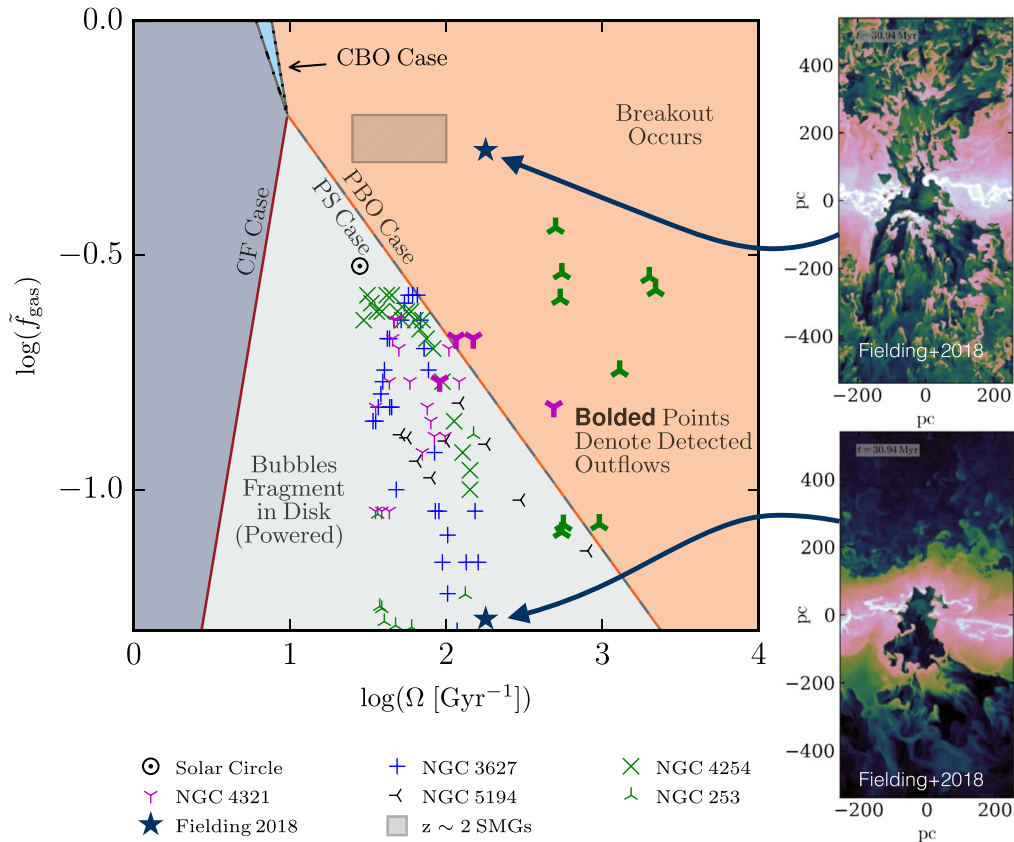
Figure 1. Gas fraction—dynamical time phase space of remnant outcomes, following Equations (9), (12), (13), and (15) from O21. Low-redshift observations are compiled from McKee et al. (2015, Solar Circle estimate), Gallagher et al. (2018, radial gas fractions for NGCs), Leroy et al. (2015, for NGC 253 circumnuclear clump surface densities), Sorai et al. (2000, for molecular gas data in the NGC 253 disk), and rotation curves from Sofue et al. (1999), Chemin et al. (2006), and Dicaire et al. (2008). Intermediate-redshift SMG observational estimates are inferred from Tacconi et al. (2013) and Genzel et al. (2020). Bold NGC points denote detected outflows. Solid orange and light blue regions denote cases where remnants successfully break out of the disk and light-gray and blue-gray regions correspond to cases where the remnant stalls/fragments in the ISM. We also compare with superbubble simulations from Fielding et al. (2018), which overlap in their initial disk and star cluster properties with this model. *Insets at right*: these simulations are in good agreement with our model, hosting dramatic breakouts in PBO case parameter space and churning stalled bubbles in the PS case parameter space (images are of projected gas density for the simulations from Fielding et al. 2018, adapted from their paper).

into a galactic gas disk, with observations of galactic outflows/fountains and H I holes. In Section 2, we briefly reiterate our simple model for superbubbles, and the possible outcomes of the evolution of those bubbles in the ISM of galaxies. We then compare our model directly with observations and simulations in Section 3. Finally, we discuss the model in the context of star formation/galaxy evolution literature, and summarize our results in Section 4.

2. Superbubble Model, in Brief

Here we review our model (the details of which can be found in O21) for the growth and eventual outcomes of a supernova-driven superbubble following the formation of a star cluster of mass M_{cl} in a GMC. A short period after the formation of the star cluster, core-collapse SNe (hereafter referred to simply as SNe) begin to occur as the most massive stars end their lives. For our model, we assume the star cluster to form instantaneously, with a formation efficiency scaling with the local gas surface density (per the simulations of Grudić et al. 2018). Approximately $N_{SNe} \approx M_{cl}/100 \, M_\odot$ SNe detonate over a short period of $t_{SNe} \sim 40 \, \mathrm{Myr}$, with the SNe remnants overlapping to form a cavity in the ISM that expands as a superbubble. The superbubble expands until the shock front either comes into pressure equilibrium with the surrounding

ISM or breaks out of the gas disk and drives a galactic fountain/outflow (see Section 2.2). The cartoon in Figure 1 in O21 illustrates the model and general outcomes of the superbubble evolution.

2.1. Superbubble Evolution in the ISM

In O21, we considered a simplified slab geometry for the ISM with a mean mass density of $\bar{\rho}_g = \Sigma_g/2H$, where a star cluster forms at the galactic midplane with a mass $M_{cl} = \pi H^2 \Sigma_g^2/\Sigma_{crit}$ (according to Grudić et al. 2018, $\Sigma_{crit} = 2800 \, M_\odot \, \mathrm{pc}^{-2}$). To model the evolution of the superbubble, we take the bubble to be in a momentum-conserving phase, with the momentum of the shock front at a radius R_b, having swept up the mass of gas within that radius, to be $P_b = \frac{4}{3}\pi R_b^3 \bar{\rho}_g \, dR_b/dt$ (Equation (3), O21, also Fielding et al. 2018; El-Badry et al. 2019), where $dR_b/dt \equiv v_b$ is the expansion velocity of the superbubble. At all points in time, we balance this momentum with the cumulative momentum injected up until that time by SNe from the central star cluster (i. e., $P_b = P_{SNe}$). To model the rate and nominal momentum injection of SNe, we invoke a power-law delay time distribution, with $dN_{SN}/dt \propto t^{-\alpha}$ (see Appendix A of Orr et al. 2019 and O21 for a more detailed discussion; in this Letter, we take $\alpha = 0.46$) and assume that a fiducial momentum

Table 1
Superbubble Outcome Boundaries

Boundary Cases (Description)	Boundary Equation	Parametric Constraint	O21 Equation No.
PBO/PS Case ("Powered Breakout/Stall")	$\tilde{f}_g = \frac{\sqrt{2}\pi G}{3} \frac{\Sigma_{\rm crit}}{(P/m_\star)_0} \left(\frac{4\Omega t_{\rm SNe}}{2-\alpha}\right)^{1-\alpha} \frac{1}{\Omega}$	$\Omega \geqslant (2-\alpha)/4t_{\rm SNe}$	Equation (9)
PBO/CBO Case ("Powered/Coasting Breakout")	$\tilde{f}_g = \frac{\sqrt{2}\pi G}{3} \frac{\Sigma_{\rm crit}}{(P/m_\star)_0} \left(\frac{2-\alpha}{4\Omega t_{\rm SNe}}\right) \frac{1}{\Omega}$		Equation (12)
CBO/CF Case ("Coasting Breakout/Fragmentation")	$\tilde{f}_g = \frac{\sqrt{2}\pi G}{3} \frac{\Sigma_{\rm crit}}{(P/m_\star)_0} \frac{1}{\Omega}$	$\Omega \leqslant (2-\alpha)/4t_{\rm SNe}$	Equation (15)
CF/PS Case ("Coasting Fragmentation/Powered Stall")	$\tilde{f}_g = \frac{\sqrt{2}\pi G}{3} \frac{\Sigma_{\rm crit}}{(P/m_\star)_0} \left(\frac{4\Omega t_{\rm SNe}}{2-\alpha}\right)^3 \frac{1}{\Omega}$		Equation (13)

of $(P/m_\star)_0$ is injected by each SN ($\approx 3000\,{\rm km\,s^{-1}}$, Martizzi et al. 2015, normalized as 1 SN per 100 $M_\odot$). Notionally, all SNe occur over a time period $0 < t < t_{\rm SNe}$ corresponding to the time from first SNe to occur in the star cluster (lifetime of the most massive star formed) until the time of the last SNe to occur (lifetime of the least massive star to undergo a core-collapse SN, ≈ 40 Myr), which divides up our parameter space into cases where the bubble evolves with and without additional SN momentum being injected.

Balancing the bubble and feedback momenta, we found relations for the bubble radius and shock front velocity in time (Equations (7) and (8), O21):

$$\frac{R_b}{H} = \left[6\frac{\Sigma_g}{\Sigma_{\rm crit}}\frac{(P/m_\star)_0}{H/t_{\rm SNe}}\right]^{\frac{1}{4}} \begin{cases} \frac{1}{(2-\alpha)^{1/4}}\left(\frac{t}{t_{\rm SNe}}\right)^{\frac{2-\alpha}{4}} \\ \qquad\qquad 0 < t < t_{\rm SNe} \\ \left[\frac{t}{t_{\rm SNe}} - \left(\frac{1-\alpha}{2-\alpha}\right)\right]^{\frac{1}{4}} \\ \qquad\qquad t > t_{\rm SNe} \end{cases}$$

$$\frac{v_b}{\sigma} = \frac{1}{4\Omega t_{\rm SNe}}\left[6\frac{\Sigma_g}{\Sigma_{\rm crit}}\frac{(P/m_\star)_0}{H/t_{\rm SNe}}\right]^{\frac{1}{4}}$$
$$\times \begin{cases} (2-\alpha)^{\frac{3}{4}}\left(\frac{t}{t_{\rm SNe}}\right)^{-\frac{(2+\alpha)}{4}} \\ \qquad\qquad 0 < t < t_{\rm SNe} \\ \left[\frac{t}{t_{\rm SNe}} - \left(\frac{1-\alpha}{2-\alpha}\right)\right]^{-\frac{3}{4}} \\ \qquad\qquad t > t_{\rm SNe} \end{cases}$$

2.2. Superbubble Outcomes

The outcomes of the evolution of these superbubbles are broken down into four cases, depending on whether or not the bubbles break out of the disk (at a time $t_{\rm BO}$), and if the central star cluster is still producing SNe. If the superbubble comes into pressure equilibrium with the surrounding ISM (for a turbulent ISM, $P_{\rm ISM} \sim \bar{\rho}_g\sigma^2$), it will not maintain coherence in its expansion to reach the gas-disk scale height, and instead the shock front will fragment/stall (as shown in the simulations by Fielding et al. 2018). Thus, we take the superbubbles to stall and fragment when $v_b \approx \sigma$, demarcating the difference between cases where the remnant successfully and unsuccessfully reaches the disk scale height.

We considered the following cases in O21,

PBO Case: "Powered Breakout," SNe remnant superbubble reaches the gas-disk scale height, $R_b = H$, *before* the central star cluster ceases producing SNe, $t_{\rm BO} < t_{\rm SNe}$.

CBO Case: "Coasting (unpowered) Breakout," remnant reaches the gas disk scale height, $R_b = H$, *after* the central star cluster ceases producing SNe, $t_{\rm BO} > t_{\rm SNe}$.

CF Case: "Coasting (unpowered) Fragmentation," the remnant fragments in the turbulent ISM (i.e., the velocity of the shock front falls below the turbulent velocity of the ISM), $v_b < \sigma$, *before* reaching the gas disk scale height, $R_b(v_b = \sigma) < H$, *after* the central star cluster ceases producing SNe, $t(v_b = \sigma) > t_{\rm SNe}$.

PS Case: "Powered Stall," bubble expansion stalls in the turbulent ISM, $v_b < \sigma$, *before* reaching the gas-disk scale height, $R_b(v_b = \sigma) < H$, *before* the central star cluster ceases producing SNe, $t(v_b = \sigma) < t_{\rm SNe}$.

Following our assumptions regarding star cluster formation efficiency, and that locally, gas in galaxies finds itself marginally stable against gravitational fragmentation and collapse with Toomre-$\tilde{Q}_{\rm gas} \approx 1$, we found in O21 that the boundaries between these four cases could be entirely expressed in terms of local gas fraction $\tilde{f}_g \equiv \Sigma_g/(\Sigma_g + \Sigma_\star)$ and inverse dynamical time $\Omega \equiv v_c/R$. We refer to Table 1 for the boundaries between cases, in $\tilde{f}_g$–Ω space, along with the constraints in Ω derived in O21 (and referencing Equation numbers therein).

3. Comparison to Observations

We compare our model with observational data for the solar circle and low-redshift NGCs 253, 3627, 4254, 4321, and 5194 (M51) in Figure 1. Combining the spatially resolved molecular gas surface-density data set from Gallagher et al. (2018) taken with ALMA for the NGCs (except for NGC 253, for which we take ALMA molecular gas data from Leroy et al. 2015 of the star-forming clumps in its circumnuclear region, and Nobeyama Radio Observatory CO data from Sorai et al. 2000 for its disk), from which we derive (azimuthally averaged) radial gas-fraction profiles calculated from their data as $\tilde{f}_{\rm gas} \equiv (\Sigma_{\rm mol} + \Sigma_{\rm H\,I})/(\Sigma_{\rm mol} + \Sigma_{\rm H\,I} + \Sigma_\star)$ where $\Sigma_{\rm mol}$ is the molecular gas-surface density and $\Sigma_{\rm H\,I}$ is the atomic-hydrogen surface density. Gallagher et al. (2018) references Querejeta et al. (2015) for radial stellar surface-density profiles, whereas we use J- and Ks-band VISTA data from Iodice et al. (2014) to estimate $\Sigma_\star$ at the location of the star-forming circumnuclear observed by Leroy et al. (2015), and stellar disk parameters from Bland-Hawthorn et al. (1997) for the
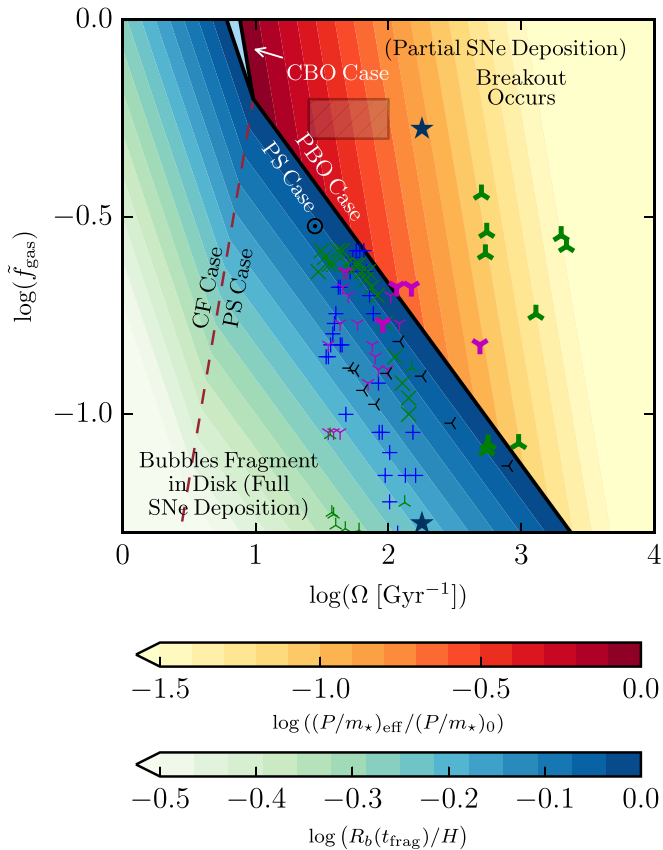
Figure 2. Fragmentation radius as a fraction of disk scale height (for CF/PS cases), and ratio of "effective" to fiducial feedback strength of superbubbles that break out of the disk *before* t_{SNe} (PBO case) in gas fraction—dynamical time phase space. We color the parameter space by predictions from Equations (17), (18), and (20) in O21, and include the same observational data and case boundary lines as in Figure 1. The light blue region denotes the CBO case where remnant coasts out of the disk but deposits all feedback momentum into the dense gas. Dashed cardinal line indicates division between the CF (coasting fragmentation) and PS (powered stall) cases. We find good agreement with the breakout time and fragmentation scale of the simulations by Fielding et al. (2018). Low-redshift observations suggest that superbubbles in the local universe fragment very near the gas disk scale height (i. e., $R_b(t_{frag})/H \gtrsim 0.7$) and that those which break out deposit as little as ~10% of feedback momentum *locally* into dense gas. Whereas, $z \sim 2$ galaxies (hatched gray patch) may deposit the majority of their feedback momentum into the ISM, suggesting that the effects of breakout may be significantly different in high-redshift hosts.

disk of NGC 253. The Gallagher et al. (2018) data set extends $R = 0$–6 kpc radially (radial bin sizes range from ~180–570 pc in width), and so does not extend into the atomic gas-dominated galactic outskirts of any of these galaxies (where dynamical times grow long; see discussion in second half of Section 4.1). For NGC 253, the disk data from Sorai et al. (2000) has $R = 0$–5 kpc with $\Delta R \approx 200$ pc, and the observations of circumnuclear clumps (from Leroy et al. 2015) have $R < 1$ kpc with $\Delta R \sim 30$ pc. For comparison with our model, we then interpolate the rotation curves for these galaxies measured by Chemin et al. (2006) and Dicaire et al. (2008) to produce inverse orbital dynamical times Ω. Estimates for the solar circle ($\Sigma_\star \approx 35\ M_\odot$, $\Sigma_{gas} \approx 15\ M_\odot$, and $\Omega \approx 35\ \mathrm{Gyr}^{-1}$) are taken from McKee et al. (2015).

Nearly all of the nearby galaxies (and the solar circle) fall into the parameter space of the PS case, with the exception of the central regions ($\lesssim 1$ kpc) of NGCs 253 and 4321, which fall into the PBO case ("Powered Breakout"). None of NGCs 3627, 4254, or 5194 (or the solar circle) have significantly detected SN-driven outflows (Calzetti et al. 2005; Weżgowiec et al. 2012; Law et al. 2018). It is difficult to find studies reporting nondetections of outflows (e.g., in NGC 3627 and 5194, we find many reports of gas and star formation rate distributions but no studies of outflow properties), however, for NGC 4254, Weżgowiec et al. (2012) reports that a relatively homogenous hot gas distribution (inferred from X-ray emission) disfavors significant star-formation-driven outflows. However, there *is* evidence of an outflow originating from the circumnuclear region of NGC 4321 (Castillo-Morales et al. 2007, supported blueshifted interstellar contamination of NaD absorption in their data). And NGC 253 hosts a notable superwind, driven by its central starburst (Bolatto et al. 2013, seen as a wide-velocity component molecular CO wind originating from the central starburst). The predicted PBO/PS case boundary is thus consistent with observations in nearby star-forming galaxies with our fiducial parameters. That the observational data fall nearly along the powered breakout/fragmentation boundary is also consistent with the picture that superbubbles are by and large driving turbulence in galaxies at or near the (gas) disk scale height (see Section 3.1 for discussion).

We also include observational estimates for $z \sim 2$ star-forming submillimeter galaxies (SMGs), as a hatched gray region. To compile this data, we combined rotation curve data from Genzel et al. (2020) with (radial) positions of star-forming clumps in a subset of those galaxies from Förster Schreiber et al. (2011) for a range of $\Omega \sim 25$–$100\ \mathrm{Gyr}^{-1}$, and then estimates for a range of gas fractions from Tacconi et al. (2013) of $\tilde{f}_g \sim 0.5$–0.7. For nearly any reasonable range of physical parameters, the $z \sim 2$ SMGs appear to fall in the PBO case regime, commensurate with the observed ubiquity of outflows in the intermediate-redshift universe (Weiner et al. 2009). Furthermore, the transition from galaxies having pervasive dramatic outflows to relatively rarely hosting them may be more a matter of falling local gas fractions than an evolution in Ω.

Lastly, we include two data points from simulations by Fielding et al. (2018). These simulations are of a stratified turbulent disk, with $\Sigma_g = 30$ and $300\ M_\odot\ \mathrm{pc}^{-2}$, an effective disk-surface density of $\Sigma_{disk} \approx 570\ M_\odot\ \mathrm{pc}^{-2}$, and an inverse dynamical time of $\Omega \approx 175\ \mathrm{Gyr}^{-1}$. They span a range of star cluster masses, but we compare with two that fall on the star cluster formation efficiency scaling utilized by our model, namely $M_{cl} = 10^4\ M_\odot$ (when $\Sigma_g = 30\ M_\odot\ \mathrm{pc}^{-2}$) and $M_{cl} = 10^6\ M_\odot$ (when $\Sigma_g = 300\ M_\odot\ \mathrm{pc}^{-2}$). These two simulations fall squarely into PS and PBO case parameter space, respectively, and exhibit the behavior that we expect: the $M_{cl} = 10^4\ M_\odot$ cluster (with its $\Sigma_g = 30\ M_\odot\ \mathrm{pc}^{-2}$ gas surface density) stalls and fragments in the disk, sputtering at times; whereas the $M_{cl} = 10^6\ M_\odot$ cluster ($\Sigma_g = 300\ M_\odot\ \mathrm{pc}^{-2}$) quickly and dramatically breaks out of the disk. We include images of the projected gas density late in the evolution of these two simulations as insets in Figure 1, adapted from their paper.

3.1. Predicting Turbulence Driving Scale and Effective Strength of Feedback in Observed Galaxies

Here we predict the local turbulence driving scale from the fragmentation of superbubbles within the ISM and *effective* strength of feedback in regions that host bubble breakout for

observed galaxies. In O21, we calculated the fragmentation/stall radius for bubbles in the CF/PS case and found (Equations (17) and (18), O21),

$$
\frac{R_b(t_{\mathrm{frag}})}{H} =
\begin{cases}
\left[\dfrac{(P/m_\star)_0}{\Sigma_{\mathrm{crit}}}\dfrac{3\Omega\tilde{f}_g}{\sqrt{2}\,\pi G}\right]^{\frac{1}{3}} & \textbf{CF Case}\\[2ex]
\left[\dfrac{(P/m_\star)_0}{\Sigma_{\mathrm{crit}}}\dfrac{3\Omega\tilde{f}_g}{\sqrt{2}\,\pi G}\right]^{\frac{1}{2+\alpha}}\\[2ex]
\quad\times\left(\dfrac{2-\alpha}{4\Omega t_{\mathrm{SNe}}}\right)^{\frac{1-\alpha}{2+\alpha}} & \textbf{PS Case}
\end{cases}
$$

Similarly, we predicted the *effective* strength of feedback, $(P/M_\star)_{\mathrm{eff}}$, i.e., the fraction of momentum deposited into the ISM versus lost to outflows in the event that the superbubble were to break out of the ISM (PBO case), and found (Equation (20), O21),

$$
\frac{(P/m_\star)_{\mathrm{eff}}}{(P/m_\star)_0} = \left[\frac{\sqrt{2}\,\pi G}{3}\frac{\Sigma_{\mathrm{crit}}}{(P/m_\star)_0}\frac{2-\alpha}{4\Omega t_{\mathrm{SNe}}}\frac{1}{\tilde{f}_g\Omega}\right]^{\left(\frac{1-\alpha}{2-\alpha}\right)}.
$$

This necessarily would affect the slope of the Kennicutt–Schmidt (KS) relation Kennicutt & Evans (2012), in a feedback-regulated framework (e.g., Faucher-Giguere et al. 2013), for ISM patches in PBO parameter space.

Figure 2 shows the $\tilde{f}_g$–Ω parameter space of superbubble outcomes colored by the predicted fragmentation radius and *effective* strength of feedback, for their appropriate cases, with the same observations as Figure 1. We predict that for local star-forming galaxies (and the conditions of the solar circle), most superbubbles which do not break out of the ISM nevertheless still grow to an appreciable fraction of the gas scale height $(R_b(t_{\mathrm{frag}})/H \gtrsim 0.7)$. Indeed this might be an expected attractor state, as if the gas scale height is to be set by turbulence, and the vertical turbulent field is to be driven by SNe, then we ought to expect that SNe have a turbulence driving scale of roughly the scale height.

We see that interestingly, the *effective* strength of feedback is perhaps not dramatically reduced in $z \sim 2$ galaxies, but for local supernova-driven outflows, we predict that, e.g., NGC 253 might have only $\sim$10% of the feedback momentum from the central starburst deposited into its ISM. This suggests that although outflows might be *ubiquitous* at cosmic noon, their effects are significantly different in regards to the ability to locally regulate the ISM.

Comparing to the simulations of Fielding et al. (2018) that fall in the PS and PBO cases, respectively, we also find satisfactory agreement with our predictions. Their simulated superbubble that failed to break out grew to $\sim$0.9H, before fragmenting and churning with a relative size of $\sim$0.7–0.8H, and the simulation that successfully broke out did so after approximately $\sim$2–3 Myr. This fragmentation scale was slightly larger than we predict here, but their numerical setup slightly differed from our model assumptions, having a vertically stratified inhomogeneous ISM and flat ($\alpha = 0$) SNe time distribution, which may account for the difference. In the case of the successful breakout simulation, their flat SNe time distribution and $t_{\mathrm{SNe}} \approx 30$ Myr may account for the difference between our predicted $(P/m_\star)_{\mathrm{eff}}$ and the simulation (see Equation (19), O21).
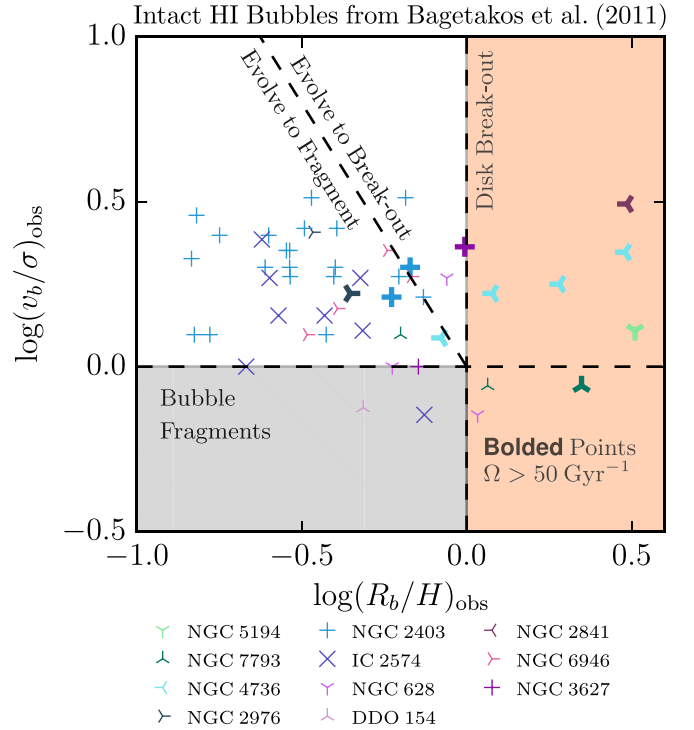

Figure 3. Observed properties of "intact" H I bubbles from (Bagetakos et al. 2011, using THINGS rotation curves from de Blok et al. 2008 to estimate H) in local star-forming galaxies, and their predicted outcomes. Orange and hatched gray regions denote parameter space where the bubbles are expected to have broken out of the ISM disk ($R_b > H$) or fragmented within it ($v_b < \sigma$), respectively. Bubble radii and velocities (Equations (7) and (8) O21, see also Section 2.1) are predicted to evolve in $\log v_b/\sigma$-$\log R_b/H$ along lines of constant slope ($-(2+\alpha)/(2-\alpha)$ in log–log space). The dashed line in the "evolving bubbles" portion of parameter space demarcates the superbubbles we predict will fragment within the ISM (PS case) from those that this model predicts will break out of the local gas disk (PBO case). Bolded points indicate superbubbles in regions with inverse dynamical times $\Omega > 50$ Gyr^{-1} (or $t_{\mathrm{dyn}} < 20$ Myr $= t_{\mathrm{SNe}}/2$), showing that almost all of the "largest" bubbles (relative to local H) have short dynamical times (i.e., in the central regions of galaxies).

3.2. Comparing to Observed H I Holes & Bubbles

In Figure 3, we plot observed H I bubble radii and expansion velocities from local star-forming galaxies in the THINGS survey by Bagetakos et al. (2011, we used THINGS rotation curves from de Blok et al. 2008 to estimate local H) to interpret the likely outcome of these bubbles. Bagetakos et al. (2011) identified gaps and voids in spatially and velocity-resolved data of the THINGS H I disks, fitting ellipsoids to find H I bubble sizes and expansion velocities. Their sample was divided up into three types of H I bubble; here we consider only their *type 3*, where the bubble is still intact with both near and far edges detected, comparable with still-evolving superbubbles in our model.

Predicting whether or not we expect an observed superbubble to fragment or breakout is possible when considering the $t < t_{\mathrm{SNe}}$ cases of Equations (7) and (8) of O21 (see Section 2.1). Taking the ratio v_b/R_b, we find that this evolves as $v_b \propto R_b^{-(2+\alpha)/(2-\alpha)}$. And so, bubbles observed to be below a line of this constant slope divide the v_b–R_b space into bubbles that we expect to fragment and those that we expect to break out.

The observed bubbles whose radii appear to already be greater than H all come from short dynamical time regions,

where $1/\Omega = t_{\rm dyn} < 20\,{\rm Myr} = t_{\rm SNe}/2$. This suggests that the H I bubbles are remaining fairly coherent after they have already broken out of the galactic nuclei, or that we are systematically underestimating H in these regions. A number of these bubbles are in the inner ring of NGC 4736, which appears to be a dynamically induced starburst (Munoz-Tunon et al. 2004), for which our assumption of $\tilde{Q}_{\rm gas} \approx 1$ may not hold. As well, identifying *intact* H I bubbles here may be problematic given the predominantly molecular nature of the central regions of local $L_\star$ star-forming galaxies (Jiménez-Donaire et al. 2019).

Considering the observed intact bubbles from regions with $\Omega < 50\,{\rm Gyr}^{-1}$ (for $v_c \approx 200\,{\rm km\,s}^{-1}$, this is $R > v_c/\Omega \approx 4\,{\rm kpc}$), the ensemble of radii and expansion velocities suggests that all of these H I bubbles will eventually fragment in the ISM rather than drive significant outflows/fountains. This is consistent with the $\tilde{f}_{\rm gas}$-Ω profiles of local star-forming galaxies (see Figure 1), where the only regions that host superbubble breakout are the central starbursts (where various gas dynamics have fed the formation of central super star clusters).

4. Discussion & Summary

4.1. The Extreme Rarity of Coasting Outcomes

As discussed in Section 3.4 of O21, the primary difficulty in realizing coasting (CBO and CF cases) outcomes appears to lie in the fact that the star-forming extent of the vast majority of galaxies does not reach so far out (radially) to have dynamical times exceeding a 100 Myr (i.e., $1/t_{\rm dyn} = \Omega = 10\,{\rm Gyr}^{-1}$). For the most part, rotation curves in galaxies are sufficiently high, and their star-forming edges sufficiently close, that dynamical times remain shorter than $4t_{\rm SNe}/(2-\alpha)$, and only *powered* outcomes are seen. The only exceptions may be in ultra-diffuse dwarfs (UDGs), having low v_c and large extents (Beasley et al. 2016). Even then, this model is only relevant for those that still maintain some star-forming gas (improbable for UDGs).

4.2. Alternative Cluster Formation Model: Constant Star Cluster Formation Efficiency

Alternative models for star cluster formation efficiency have been proposed, arguing that star formation proceeds at a constant efficiency of roughly 1% per freefall time (Krumholz & Tan 2007; see Krumholz et al. 2019 for a review of (low) star formation efficiency in clusters). If we were to adopt a constant efficiency per Toomre-mass model, as opposed to the Grudić et al. (2018) model, where $M_{\rm cl} = \epsilon_{\rm cl} M_g \approx \epsilon_{\rm cl} \pi H^2 \Sigma_g$, where $\epsilon_{\rm cl} = 0.01$, and holding the rest of the model fixed, then throughout the text the only difference required would be to replace $\Sigma_{\rm crit} \to \Sigma_g/\epsilon_{\rm cl}$. Whereupon, we would plot all our figures in $\tilde{f}_g/\Sigma_g$-Ω space, rather than $\tilde{f}_g$-Ω space. The rest of the results and analysis would remain unchanged. Figure 4 shows the case boundaries in the somewhat unusual $\tilde{f}_g/\Sigma_g$-Ω space.

The main difference of this alternative model is that breakout is now dependent on the local *disk* surface density, as $\Sigma_{\rm disk} \approx \Sigma_\star + \Sigma_g = \Sigma_g/\tilde{f}_g$. In fact, such a model would imply that breakout only occurs at lower (relatively speaking) disk surface densities for a given local dynamical time: above a local disk surface density, the resulting superbubble is effectively smothered by the disk. At the critical dynamical time (where all four case boundaries intersect) this local disk surface density is $\approx 45\,M_\odot\,{\rm pc}^{-2}$, and it grows to ≈ 130 $M_\odot\,{\rm pc}^{-2}$ at $\Omega = 10^2$ ${\rm Gyr}^{-1}$. Given that regions with shorter dynamical times are generally coreward in disk galaxies, and
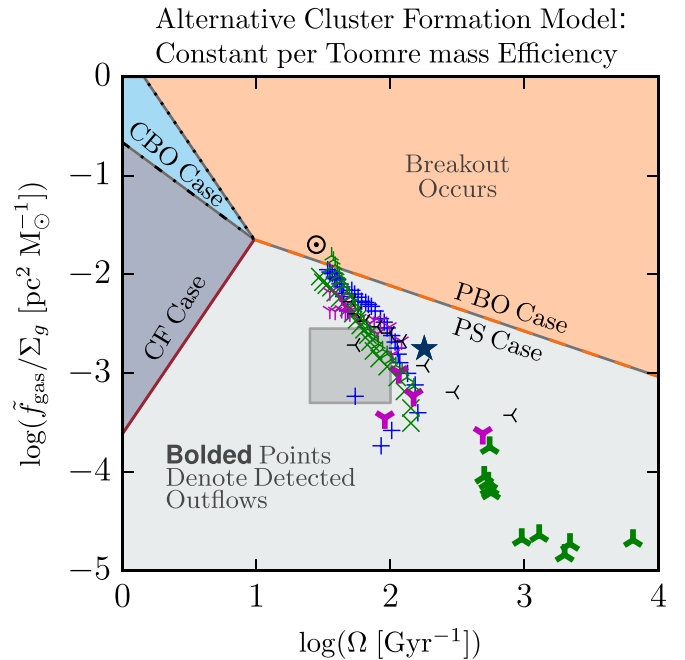

Figure 4. Case boundaries with constant star cluster formation efficiency (per Toomre-mass) assumed for the superbubble model, in the style of Figure 1, in inverse disk surface density–dynamical time phase space, following required adjustments to Equations (9), (12), (13), and (15). In replacing $\Sigma_{\rm crit} \to \Sigma_g/\epsilon_{\rm cl}$, the adjustment to the case boundaries is found by substituting $\tilde{f}_g \to \tilde{f}_g/\Sigma_g$ (i.e., $1/\Sigma_{\rm disk}$). With a constant star cluster formation efficiency, CBO/CF cases remain unlikely to occur given the long dynamical times required (unchanged from fiducial model predictions). In this case, our fiducial model parameters and $\epsilon_{\rm cl} = 0.01$ predict that breakout occurs at lower disk surface densities (almost always $<130\ M_\odot\,{\rm pc}^{-2}$), implying that breakout, i.e., outflows/fountains never occur in the inner disk, contrary to observations. In spite of the outflow detection in NGC 4321 by Castillo-Morales et al. (2007), and the well-known superwind of NGC 253, we would not predict the centers of either NGC 253 or 4321 to host a SN-driven outflow. Instead, this constant efficiency model predicts outflows from solar circle (and more diffuse) disk conditions. Moreover, we would also expect the surface densities in high-redshift SMGs to be such that there are no predicted outflows, contrary to observations from $z \sim 1$–3.

that generally the disk (stellar + gaseous) surface densities of the central regions in Milky Way mass galaxies greatly exceed $100\ M_\odot\,{\rm pc}^{-2}$ (see the PHANGS-ALMA sample of Sun et al. 2020), this model suggests that superbubble breakout, and thus outflows, would not occur in the inner disk regions of galaxies, only in their outskirts. This is contrary to many observations of galactic winds and outflows, specifically those of galaxies without AGN, which nonetheless tend to report outflows and fountains originating from the inner regions of galaxies (e.g., Bolatto et al. 2013). Consequently, these data disfavor a constant (per Toomre-mass) star cluster formation efficiency within this superbubble feedback model.

4.3. Summary

In this Letter, we compared a model (derived in O21) of clustered SNe feedback in disk environments with observations of local and high-redshift star-forming galaxies. Of specific interest, we tested our predictions from O21 of the ability of supernova-driven superbubbles to break out of the gas disk of a galaxy with known hosts of superwinds, and galaxies thought to lack them. As well, we examined observed H I bubbles/holes in the context of our predicted scalings for bubble radii and velocities.

Key takeaways from comparing this model to observations include:

1. Spatially resolved observations of $z \approx 0$ star-forming galaxies suggest that most star-forming regions in the local universe fall into the "PS case," i.e., that superbubbles stall and fragment inside the disk and locally deposit almost all of their momentum. Higher-redshift observations suggest that $z \sim 2$ SMGs exist in "PBO case" parameter space, i.e., superbubbles at $z \sim 2$ are (always) able to drive outflows/fountains. The central regions of some local galaxies also appear to lie in the predicted "PBO case" region (e.g., NGC 4321, which has evidence of central star-formation-driven winds). The transition from high to low redshift galaxies, in terms of hosting pervasive outflows to only those in circumnuclear regions, appears driven by an evolution from high to low local gas fractions in star-forming regions according to this model.

2. Observed intact H I bubble radii and velocities in local star-forming galaxies (from Bagetakos et al. 2011) are consistent with the $\tilde{f}_{gas}$-Ω profile interpretations: most feedback driven bubbles in local galaxies should fragment inside the ISM, and that those able to break out originate from short dynamical time regions in the nuclear regions.

3. A cluster formation model that includes a constant star formation efficiency per Toomre mass is effectively ruled out by the observational data (see Section 4.2), as this model predicts that high surface density regions (e.g., high-redshift star-forming clumps or low-redshift circumnuclear regions) would be unable to host superbubbles capable of breaking out and driving outflows/fountains.

In comparing to observations, we find that the clustering of SNe indeed has important implications for the local efficacy of star formation, and the evolution of galaxies more broadly across cosmic time. Future highly spatially resolved observations, capable of identifying and quantifying the properties of supernova-driven superbubbles, especially in dense molecular gas structures, should help to further constrain the effective strength of feedback under varying local galactic conditions and inform subgrid models for feedback in cosmological galaxy simulations.

ORCID iDs

Matthew E. Orr https://orcid.org/0000-0003-1053-3081
Drummond B. Fielding https://orcid.org/0000-0003-3806-8548
Christopher C. Hayward https://orcid.org/0000-0003-4073-3236
Blakesley Burkhart https://orcid.org/0000-0001-5817-5944

References

Agertz, O., & Kravtsov, A. V. 2016, ApJ, 824, 79
Bagetakos, I., Brinks, E., Walter, F., et al. 2011, AJ, 141, 23
Beasley, M. A., Romanowsky, A. J., Pota, V., et al. 2016, ApJL, 819, L20
Behroozi, P. S., Wechsler, R. H., & Conroy, C. 2013, ApJL, 762, L31
Bland-Hawthorn, J., Freeman, K. C., & Quinn, P. J. 1997, ApJ, 490, 143
Bolatto, A. D., Warren, S. R., Leroy, A. K., et al. 2013, Natur, 499, 450
Burkhart, B., & Mocz, P. 2019, ApJ, 879, 129
Calzetti, D., Kennicutt, R. C., Jr., Bianchi, L., et al. 2005, ApJ, 633, 871
Castillo-Morales, A., Jiménez-Vicente, J., Mediavilla, E., & Battaner, E. 2007, MNRAS, 380, 489
Chemin, L., Balkowski, C., Cayatte, V., et al. 2006, MNRAS, 366, 812
Dale, J. E., Ngoumou, J., Ercolano, B., & Bonnell, I. A. 2014, MNRAS, 442, 694
de Blok, W. J. G., Walter, F., Brinks, E., et al. 2008, AJ, 136, 2648
Dicaire, I., Carignan, C., Amram, P., et al. 2008, MNRAS, 385, 553
El-Badry, K., Ostriker, E. C., Kim, C.-G., Quataert, E., & Weisz, D. R. 2019, MNRAS, 490, 1961
Faucher-Giguere, C.-A., Quataert, E., & Hopkins, P. F. 2013, MNRAS, 433, 1970
Fielding, D., Quataert, E., & Martizzi, D. 2018, MNRAS, 481, 3325
Fielding, D. B., & Bryan, G. L. 2021, arXiv:2108.05355
Förster Schreiber, N. M., Shapley, A. E., Genzel, R., et al. 2011, ApJ, 739, 45
Gallagher, M. J., Leroy, A. K., Bigiel, F., et al. 2018, ApJ, 858, 90
Genzel, R., Price, S. H., Übler, H., et al. 2020, ApJ, 902, 98
Grudić, M. Y., Hopkins, P. F., Faucher-Giguère, C.-A., et al. 2018, MNRAS, 475, 3511
Hopkins, P. F., Wetzel, A., Kereš, D., et al. 2018, MNRAS, 480, 800
Iodice, E., Arnaboldi, M., Rejkuba, M., et al. 2014, A&A, 567, A86
Jiménez-Donaire, M. J., Bigiel, F., Leroy, A. K., et al. 2019, ApJ, 880, 127
Kennicutt, R. C., & Evans, N. J. 2012, ARA&A, 50, 531
Kim, C.-G., & Ostriker, E. C. 2017, ApJ, 846, 133
Koo, B.-C., & McKee, C. F. 1992, ApJ, 388, 103
Krumholz, M. R., Burkhart, B., Forbes, J. C., & Crocker, R. M. 2018, MNRAS, 477, 2716
Krumholz, M. R., McKee, C. F., & Bland-Hawthorn, J. 2019, ARA&A, 57, 227
Krumholz, M. R., & Tan, J. C. 2007, ApJ, 654, 304
Lada, C. J., & Lada, E. A. 2003, ARA&A, 41, 57
Law, C. J., Zhang, Q., Ricci, L., et al. 2018, ApJ, 865, 17
Leroy, A. K., Bolatto, A. D., Ostriker, E. C., et al. 2015, ApJ, 801, 25
Li, H., Vogelsberger, M., Marinacci, F., & Gnedin, O. Y. 2019, MNRAS, 487, 364
Martizzi, D., Faucher-Giguere, C.-A., & Quataert, E. 2015, MNRAS, 450, 504
Martizzi, D., Fielding, D., Faucher-Giguère, C.-A., & Quataert, E. 2016, MNRAS, 459, 2311
McKee, C. F., Parravano, A., & Hollenbach, D. J. 2015, ApJ, 814, 13
Munoz-Tunon, C., Caon, N., & Aguerri, J. A. L. 2004, AJ, 127, 58
Murray, N., Quataert, E., & Thompson, T. A. 2010, ApJ, 709, 191
Orr, M. E., Fielding, D. B., Hayward, C. C., & Burkhart, B. 2021, arXiv:2109.14656
Orr, M. E., Hayward, C. C., Hopkins, P. F., et al. 2018, MNRAS, 478, 3653
Orr, M. E., Hayward, C. C., & Hopkins, P. F. 2019, MNRAS, 486, 4724
Orr, M. E., Hayward, C. C., Medling, A. M., et al. 2020, MNRAS, 496, 1620
Pillepich, A., Springel, V., Nelson, D., et al. 2018, MNRAS, 473, 4077
Querejeta, M., Meidt, S. E., Schinnerer, E., et al. 2015, ApJS, 219, 5
Sofue, Y., Tutui, Y., Honma, M., et al. 1999, ApJ, 523, 136
Sorai, K., Nakai, N., Kuno, N., Nishiyama, K., & Hasegawa, T. 2000, PASJ, 52, 785
Sun, J., Leroy, A. K., Schinnerer, E., et al. 2020, ApJL, 901, L8
Tacconi, L. J., Neri, R., Genzel, R., et al. 2013, ApJ, 768, 74
Weiner, B. J., Coil, A. L., Prochaska, J. X., et al. 2009, ApJ, 692, 187
Wetzel, A. R., Hopkins, P. F., Kim, J.-h., et al. 2016, ApJL, 827, L23
Weżgowiec, M., Bomans, D. J., Ehle, M., et al. 2012, A&A, 544, A99